**Atmospheric
Chemistry
and Physics**

Corrigendum to

"Influence of Giant CCN on warm rain processes in the ECHAM5 GCM" published in Atmos. Chem. Phys., 8, 2949–2963, 2008

R. Posselt and U. Lohmann

Institute for Atmospheric and Climate Science, ETH Zurich, Universitaetsstrasse 16, 8092 Zurich, Switzerland

In the simulations for the paper "Influence of Giant CCN on warm rain processes in the ECHAM5 GCM" by Rebekka Posselt and Ulrike Lohmann (Atmos. Chem. Phys., 8, 2949–2963, 2008) we discovered that the pre-industrial (PI) simulations included only the effect of pre-industrial sulphate. All other emissions were by mistake present-day (PD). Thus, the reported values for the aerosol indirect effect (AIE) have to be corrected and the conclusions regarding the effect of the giant cloud condensation nuclei (GCCN) on the AIE change slightly. The present-day simulations are correct and thus the conclusions regarding this part are not affected.

The corrected figures (Figs. 11, 12, 13) and table (Table 5) appear below. In most cases only the numbers change but the explanation remain the same. Cases where the effect of GCCN on anthropogenic aerosols also changes are discussed below.

The changes of the zonal mean GCCN concentration as well as GCCN fraction from the pre-industrial to present-day climate are shown in Fig. 11. The GCCN concentration increases between $45° S$ and $60° N$. Below and above these latitudes the GCCN concentrations are decreasing. These changes are mostly caused by the changes in the 10 m wind speed from pre-industrial to present-day climate as shown in Fig. 12. Most obvious changes are visible in the Southern Hemisphere, where the 10 m wind speed increases between $30° S$ and $45° S$ but decreases between $45° S$ and $60° S$. In the Northern Hemisphere the 10m wind speed is slightly increasing.

The changes in the annual global and zonal means from pre-industrial to present-day climate are shown in Table 5 and Fig. 13. The increase in total cloud cover (TCC) from PI to PD decreases with an increasing amount of GCCN from 0.43 for CTL30 to 0.4 and 0.33 for simulations $GCCN_{10}$ and

$GCCN_5$, respectively. Main changes are visible in the Northern Hemisphere in analogy to the changes in total water path (TWP) and the cloud drop number concentration (N_l) of the original paper.

The decreasing TCC differences results in reduced changes in the shortwave (SW) radiation budget depending on whether and how many GCCN are present. The implementation of the prognostic rain scheme reduces the SW total anthropogenic effect by $0.29\,W\,m^{-2}$ in CTL30 and by $0.39\,W\,m^{-2}$ in CTL10 as compared to $-2\,W\,m^{-2}$ reported by Lohmann et al. (2007) for the standard ECHAM5-HAM. In case of the simulation $GCCN_{10}$ the GCCN number is not yet large enough to cause considerable changes in the SW radiation globally but in simulation $GCCN_5$ the GCCN lead to further reduction in the SW radiation by $0.28\,W\,m^{-2}$. As in the original paper, effects are largest on the Northern Hemisphere due to an enhanced aerosol and, thus, CCN number caused by industrialization in Europe, North America and Asia.

The changes in the SW radiation are also reflected in the changes of the net radiative budget. The net radiation change is $-1.52\,W\,m^{-2}$ for CTL30 and $-1.43\,W\,m^{-2}$ for CTL10 as compared to $-1.9\,W\,m^{-2}$ for the standard ECHAM5-HAM. Simulation $GCCN_{10}$ does not show a further reduction, but in simulation $GCCN_5$ the change in net radiation due to anthropogenic aerosols is reduced to $-1.28\,W\,m^{-2}$. Thus, in simulation $GCCN_5$ the GCCN are able to counteract the effects of increased aerosol loads in PD to some extend. For the simulation $GCCN_{10}$ this effect is negligible.

References

Lohmann, U., Stier, P., Hoose, C., Ferrachat, S., Kloster, S., Roeckner, E., and Zhang, J.: Cloud microphysics and aerosol indirect effects in the global climate model ECHAM5-HAM, Atmos. Chem. Phys., 7, 3425–3446, 2007, http://www.atmos-chem-phys.net/7/3425/2007/.
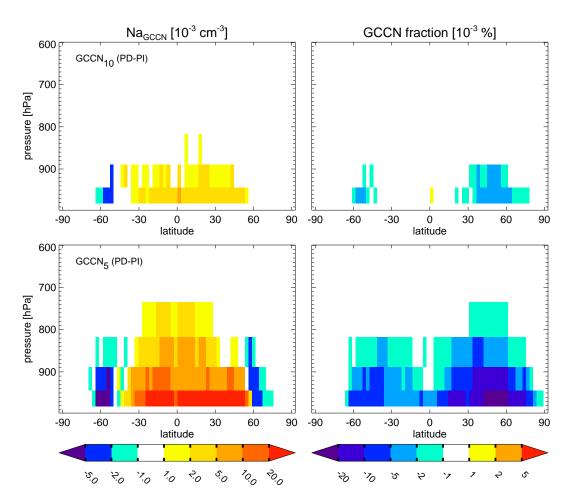
Correspondence to: R. Posselt
(rebekka.posselt@env.ethz.ch)

Fig. 11. Difference of zonal average of giant sea salt concentration and giant sea salt fraction between present-day and pre-industrial simulations of $GCCN_{10}$ (upper row) and $GCCN_5$ (lower row).
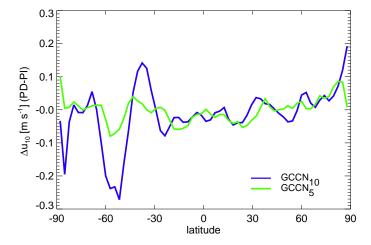

Fig. 12. Difference of 10 m wind speed between present-day and pre-industrial simulations for $GCCN_{10}$ and $GCCN_5$.
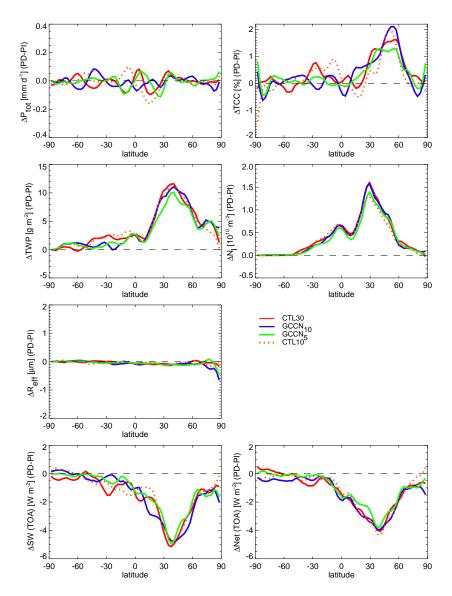
Fig. 13. Annual zonal means differences between the present-day and pre-industrial simulations of precipitation, total cloud cover, total water path, column integrated cloud droplet number, effective cloud droplet radius at cloud top (T>273.15 K) as well as short-wave and net radiation at TOA from CTL30, GCCN$_{10}$, GCCN$_5$, and CTL10 simulations.

Table 5. Annual global mean changes and interannual standard deviations of cloud properties and TOA energy budget from PD to PI.

		CTL30		GCCN$_{10}$		GCCN$_5$		CTL10	
P_{tot}	[mm d^{-1}]	-0.011	± 0.011	-0.008	± 0.006	0.008	± 0.007	-0.011	± 0.011
TCC	[%]	0.43	± 0.19	0.4	± 0.21	0.33	± 0.18	0.37	± 0.25
TWP	[g m^{-2}]	4.1	± 0.5	3.7	± 0.5	3.2	± 0.4	4.1	± 0.5
N_l	[10^{10} m^{-2}]	0.61	± 0.05	0.58	± 0.04	0.51	± 0.02	0.56	± 0.02
R_{eff}	[μm]	-0.25	± 0.04	-0.27	± 0.03	-0.25	± 0.03	-0.22	± 0.02
SW	[W m^{-2}]	-1.71	± 0.3	-1.67	± 0.27	-1.43	± 0.12	-1.61	± 0.24
LW	[W m^{-2}]	0.2	± 0.25	0.12	± 0.19	0.15	± 0.14	0.18	± 0.19
Net	[W m^{-2}]	-1.52	± 0.14	-1.55	± 0.29	-1.28	± 0.16	-1.43	± 0.15